Wind and Structures, Vol. 2, No. 4 (1999) 285-303
DOI: http://dx.doi.org/10.12989/was.1999.2.4.285

Computation of unsteady wind loading on bluff bodies using a discrete vortex method

I.J. Taylor† and M. Vezza‡

Department of Aerospace Engineering, University of Glasgow, Glasgow, G12 8QQ, Scotland, U.K.

Abstract. A discrete vortex method(DVM) has been developed at the Department of Aerospace Engineering, University of Glasgow, to predict unsteady, incompressible, separated flows around closed bodies. The basis of the method is the discretisation of the vorticity field, rather than the velocity field, into a series of vortex particles that are free to move in the flow. This paper gives a brief description of the method and presents the results of calculations on static and transversely oscillating square section cylinders. The results demonstrate that the method successfully predicts the character of the flow field at different angles of incidence for the static case. Vortex lock-in around the resonance point is successfully captured in the oscillatory cases. It is concluded that the vortex method results show good agreement, both qualitatively and quantitatively, with results from various experimental data.

Key words: vortex method; bluff bodies; square cylinder; vortex-induced vibration.

1. Introduction

The knowledge of the flow field around bluff structures is of major importance in the fields of civil and wind engineering. As modern structures become ever taller or longer, the structural response to aerodynamic forcing, due to aeroelastic phenomena such as vortex shedding, has a greater impact on the design of these structures. The loading induced by the unsteady aerodynamics and the structural response to these forces are therefore a major consideration during the design process. However, much of the analysis of bluff body flow fields and the associated aeroelastic response are based on experimental investigations of the unsteady aerodynamics from various wind tunnel tests of the structures. Despite the rapid advances in computational hardware and the development of many sophisticated numerical models in recent years, the complex flow field effectively places a limitation on the use of computational methods and analysis tools. Due to the complexity of the unsteady flow field and of the associated non-linear dynamics, there are few numerical models that have demonstrated sufficient accuracy for the results to be reliably used in the analysis of a wide range of bluff body flows. However, accurate prediction of the flow field for such problems using computational methods is becoming increasingly important, to help improve the understanding of fluid-structure interactions in bluff body flows. Although this presents a challenge to computational methods, recent developments in both software and hardware have been providing valuable insights into the

† Researcher
‡ Lecturer

nature of the flow field.

One numerical technique that has undergone significant development in recent years and has been shown to be well suited to analysing unsteady and highly separated flow fields, is the discrete vortex method. The numerical technique utilised by vortex methods is based on the discretisation of the vorticity field rather than the velocity field, into a series of vortex particles. These particles are of finite core size, each carrying a certain amount of circulation, and are tracked throughout the flow field that they collectively induce. As such, the model does not require a calculation mesh and provides a very different approach to more traditional grid based computational fluid dynamics methods. One of the main advantages of vortex methods over grid based approaches is that the Lagrangian nature of the method significantly reduces some of the problems associated with grid methods, such as numerical diffusion and difficulties in achieving resolution of small scale vortical structures in the flow. Vortex particles are naturally concentrated into areas of non-zero vorticity and enable vortex methods to capture these small scale flow structures in more detail. Dispensing with a calculation mesh also eases the task of modelling a more arbitrary range of geometries. In particular, vortex methods are well suited to the analysis of moving body problems.

A key aspect of vortex methods is how the vorticity is shed from the body surface into the flow. For sharp edged bodies, the separation of the shear layer is often fixed at the corners, and this is incorporated into some models. For example in the method of Bergstrom and Wang (1997) vortex particles are alternately released from the upstream corners of a square cylinder. Bienkiewicz and Kutz (1993) used a similar procedure for releasing vortices at a specified separation point. However, the assumption that separation from the downstream corners is a secondary consideration becomes invalid as the body moves to incidence, and for high aspect ratio bodies. A more comprehensive approach is to create vortices at the surface which satisfy the no-slip condition, first introduced by Chorin (1973). Particular versions of the surface shedding technique have since been implemented, for example by Clark and Tutty (1994), Koutmoutsakos and Leonard (1995) and Walther and Larsen (1997). Comprehensive reviews of the discrete vortex method are given in Leonard (1980), Sarpkaya (1989) and Puckett (1993).

This paper presents a two dimensional discrete vortex method(DVM) that has been developed at the Department of Aerospace Engineering, University of Glasgow. The model was originally developed to analyse dynamic stall on aerofoils undergoing a pitching motion (Lin *et al.* 1996 & 1997a, b). The research presented herein summarises part of the development and validation of the DVM for the analysis of a range of bluff body flow fields and fluid-structure interaction problems. This paper presents some of the results of the validation of the method on both static and oscillating square section cylinders. More detailed results from this validation exercise have been reported in Taylor (1999).

Comparison of the results with experimental data and with predictions from other computational methods, demonstrate the capability of the method to accurately predict the variation of the flow field around a square cylinder over a range of angles of incidence. In addition, results are presented for the square cylinder undergoing a forced transverse oscillation at various amplitudes and frequencies. The results obtained demonstrate the capability of the DVM to accurately predict the flow field around oscillating bodies, including vortex lock-in close to the resonant frequency as well as the amplitude and frequency dependency of the response. The phase angle by which the lift force leads the body displacement, is also well predicted by the

DVM and compares well to experimental data.

Future work is aimed at validating the DVM for more complex bluff geometries. In particular, ongoing work includes the analysis of suspension bridge deck sections with the aim of investigating the structural stability and to derive the critical flutter velocity of representative bridge sections.

2. Discrete vortex method

2.1. Governing equations

Two-dimensional incompressible viscous flow can be described by the vorticity-stream function form of the continuity and full viscous Navier-Stokes equations :

$$\nabla^2 \Psi = -\omega \tag{1}$$

$$\frac{D\omega}{Dt} = \nu \nabla^2 \omega \tag{2}$$

where ν is the kinematic viscosity. Vorticity, ω, is defined as the curl of the velocity (3), and a vector potential, $\vec{\Psi}$, is defined by Eq. (4).

$$\vec{\omega} = \nabla \times \vec{U} \quad \text{with} \quad \vec{\omega} = \vec{k}\,\omega \tag{3}$$

$$\vec{U} = \nabla \times \vec{\Psi}, \quad \vec{\Psi} = \vec{k}\,\Psi, \quad \nabla . \vec{\Psi} = 0 \tag{4}$$

The vorticity transport Eq. (2) defines the motion of vorticity in the flow due to convection and diffusion. The calculations are subject to boundary conditions (5) that implement the no-penetration condition, that the local normal velocity of the flow at the body surface is the same as that of the body. Also, the boundary conditions indicate that the flow in the far field is undisturbed by the vorticity shed from the body surface.

$$\boldsymbol{n} . \boldsymbol{U} = \boldsymbol{n}_i . \boldsymbol{U}_i \quad \text{and} \quad \boldsymbol{U} = \boldsymbol{U}_\infty \text{ on } S_\infty \tag{5}$$

where i is the index for the body. The no-slip condition is consistent with the velocity at a point $\boldsymbol{r}_p$ on the surface or within body i being described by

$$\boldsymbol{U}_i = \boldsymbol{U}_{ic} + \Omega_i \times (\boldsymbol{r}_p - \boldsymbol{r}_{ic}) \tag{6}$$

where $\boldsymbol{r}_{ic}$ is a fixed reference point on the body, $\boldsymbol{U}_{ic}$ is the velocity of $\boldsymbol{r}_{ic}$ and Ω_i is the rotational velocity of the body (Fig. 1). This is represented in stream function form by

$$\nabla^2 \Psi_i = -2\Omega_i \tag{7}$$

The relationship between the velocity and the vorticity has been derived by Vezza (1992), also discussed by Lin (1997b), through the application of Green's Theorem to (1) for the flow region F (Fig. 2) and (7) for the body region B_i, and combining them through the boundary conditions (Lin 1997b). The velocity field is then calculated using the Biot-Savart law, which expresses the velocity in terms of the vorticity field. For a point p outside the solid region, the velocity is given by :

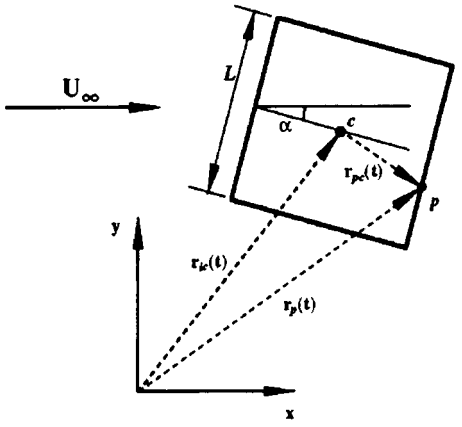

Fig. 1 Body orientation and reference coordinate system

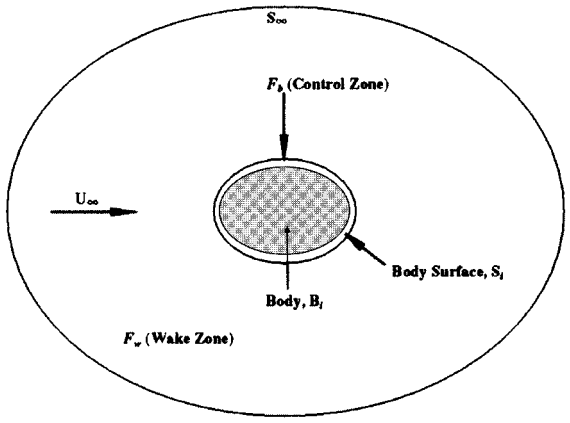

Fig. 2 Flow domain

$$\boldsymbol{U}_p = \boldsymbol{U}_\infty + \frac{1}{2\pi}\int_{F_b} \omega \frac{\boldsymbol{k}\times(\boldsymbol{r}_p - \boldsymbol{r})}{\| \boldsymbol{r}_p - \boldsymbol{r} \|^2} dF_b + \frac{1}{2\pi}\int_{F_w} \omega \frac{\boldsymbol{k}\times(\boldsymbol{r}_p - \boldsymbol{r})}{\| \boldsymbol{r}_p - \boldsymbol{r} \|^2} dF_w + \frac{1}{2\pi}\int_{B_i} 2\Omega_i \frac{\boldsymbol{k}\times(\boldsymbol{r}_p - \boldsymbol{r})}{\| \boldsymbol{r}_p - \boldsymbol{r} \|^2} dB_i \tag{8}$$

where $F = F_b \cup F_w$ and $F_b \cap F_w = 0$. Eq. (8) details the contributions to the velocity from the freestream, the nascent vorticity in the small area, F_b, around the solid region (control zone), the vorticity in the remaining flow area, F_w, and the equivalent vorticity inside the solid region due to the motion of the body, B_i.

2.2. Numerical implementation

The numerical implementation of the governing equations is presented in more detail in Lin *et al.* (1996 & 1997a, b) and Taylor (1999) with only a brief summary being presented below. The governing equations defined in the previous section are for most cases impossible to solve analytically. For this reason, an approximate solution may be obtained numerically through the discretisation of the vorticity field into a series of vortex particles. However, care must be taken that the discretisation gives a true representation of the flow domain.

For a two dimensional body, a polygonal representation of the body surface is created by connecting a series of N nodes, that define the body geometry, with straight lines forming a series of panels. Each panel is further subdivided into K equal length sub-panels. The thin area near the body surface is regarded as a special zone, the control zone, in which the vorticity is created. The vorticity in the remainder of the flow field arises through convection and diffusion of the vorticity generated in the control zone. The vorticity in the control zone can be treated as a one dimensional vortex sheet, which is then discretised using a two stage process. First, the vorticity in the control zone, γ, is treated as a quantity that varies piecewise linearly and continuously along the surface. The values of γ at the node points therefore represent the entire vorticity distribution within the control zone. Secondly, the panel distribution of vorticity is further broken down into vortex blobs, one for each sub-panel.

The γ values in the creation zone are the solution of the linear system of equations arising from the boundary conditions which are implemented by ensuring zero mass flow through each surface panel. The implementation is expressed as

$$F_{js} + F_{ji} + F_{jf} + F_{jv} + F_{jn} = 0 \tag{9}$$

where each term represents the contribution of the mass flow from different sources. The first and second terms are from the motion of the body, with the remaining terms representing the contributions from the freestream, the vortices in the wake and the nascent vortices within the control zone.

All vortices outside the control zone originate from nascent vortices, with their positions being the result of convection and diffusion at each time step. The simulation of vortex convection and diffusion employs an operator splitting technique, where the vorticity transport Eq. (2) is split into a separate convection part Eq. (10) and diffusion part Eq. (11), both of which are solved sequentially as proposed by Chorin (1973).

$$\frac{D\omega}{Dt} = 0 \tag{10}$$

$$\frac{\partial\omega}{\partial t} + \nu\nabla^2\omega \tag{11}$$

As vorticity forms one the conserved properties of the particles in inviscid flows, the velocity at the centre of each vortex particle is equal to the velocity of the vorticity transport evaluated from (8). The diffusion process is modelled using a random walk procedure (Chorin 1973) which satisfies the Gaussian distribution of zero mean and standard deviation $\sqrt{(2\Delta t/\mathrm{Re})}$, where Δt is the timestep and Re is the Reynolds number of the flow.

The calculation of the velocity of a single vortex particle requires the influence of all regions of vorticity in the flow field to be taken into account Eq. (8). For a flow field containing N particles this leads to an operation count of $O(N^2)$, which becomes prohibitive as N increases. A fast algorithm for the velocity calculation has been included in the DVM and is presented in Taylor and Vezza (1997). The procedure uses a zonal decomposition algorithm for the velocity summation and allows the effect of groups of particles on the velocity to be calculated using a single series expansion, thus significantly reducing the operation count of the calculation. The algorithm utilises a hierarchical technique similar in nature to the adaptive Fast Multipole Method (Carrier *et al.* 1988), so that the largest possible group of particles is used for each series expansion. The resulting operation count is $O(N + N\log N)$, and therefore offers a significant improvement to the calculation efficiency.

3. Results and discussion

The flow field around a square section cylinder, both static and oscillating, have been computed using the DVM. All calculations were performed using an impulsively started flow field, at a Reynolds number of 20000. A non-dimensional timestep, $\Delta tU/L$, of 0.02 was used, with the nascent vortex particles being created a distance $0.0025L$ from the surface. The body surface was represented by 160 equal length panels. The nascent vorticity was discretised using 7

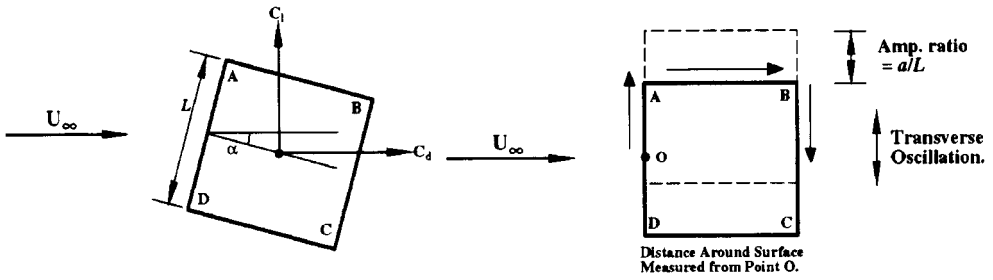

(a) Orientation of static square (b) Orientation of transversely oscillating square

Fig. 3 Orientation and labelling of square cylinder in DVM calculations

vortices per panel to ensure overlapping of the vortex cores and provide accurate resolution of the vorticity distribution on the body surface. For both the static and oscillatory cases, typical results are presented, showing comparisons with experimental data and results from other computational methods. The Reynolds number chosen for the computations was representative of the range of experimental values, which were of order 10^4 to 10^5. In addition, the experiments were carried out in smooth flow, with turbulence levels predominantly below 0.1%. The configuration of the cylinder in both the static and oscillating cases, along with the direction of the aerodynamic loads are shown in Fig. 3. A more detailed discussion of these results is given by Taylor (1999).

3.1. Static body results

3.1.1. General flow field visualisation

Figs. 4 and 5 show the flow field around the square section cylinder at two different angles of incidence. In each case, the flow at various stages of the vortex shedding cycle are shown, using the distribution of particles from the DVM, accompanied by velocity vector plots to give more clarity to the predicted flow field. In general, the qualitative prediction of the flow fields are good. The alternate vortex shedding from the body, giving rise to a classical vortex street, can clearly be seen in the 0° case (Fig. 4). At 15° incidence, the shear layer separating from the front lower corner of the body, is clearly shown to be reattaching on the lower side face (Fig. 5). The effect that this reattachment has on the mean force coefficients will be discussed in more detail in the next section. The differences in the wake structure between the two cases can clearly be discerned, with noticeably weaker vortex shedding in the 15° case.

3.1.2. Mean aerodynamic force coefficients : C_D and C_L

The mean aerodynamic force coefficients, C_L and C_D at angles of incidence ranging from $\alpha = 0°$ to 45° are compared with experimental data in Figs. 6 and 7. The correct variation of both C_L and C_D with incidence is predicted, and the results show good quantitative agreement with various experimental data. Other computational results (Bienkiewicz *et al.* 1990), in particular, do not capture the variation in the lift and drag, at the higher angles of incidence.

As the angle of incidence increases, the mean C_D reduces, primarily due to the shear layer that is

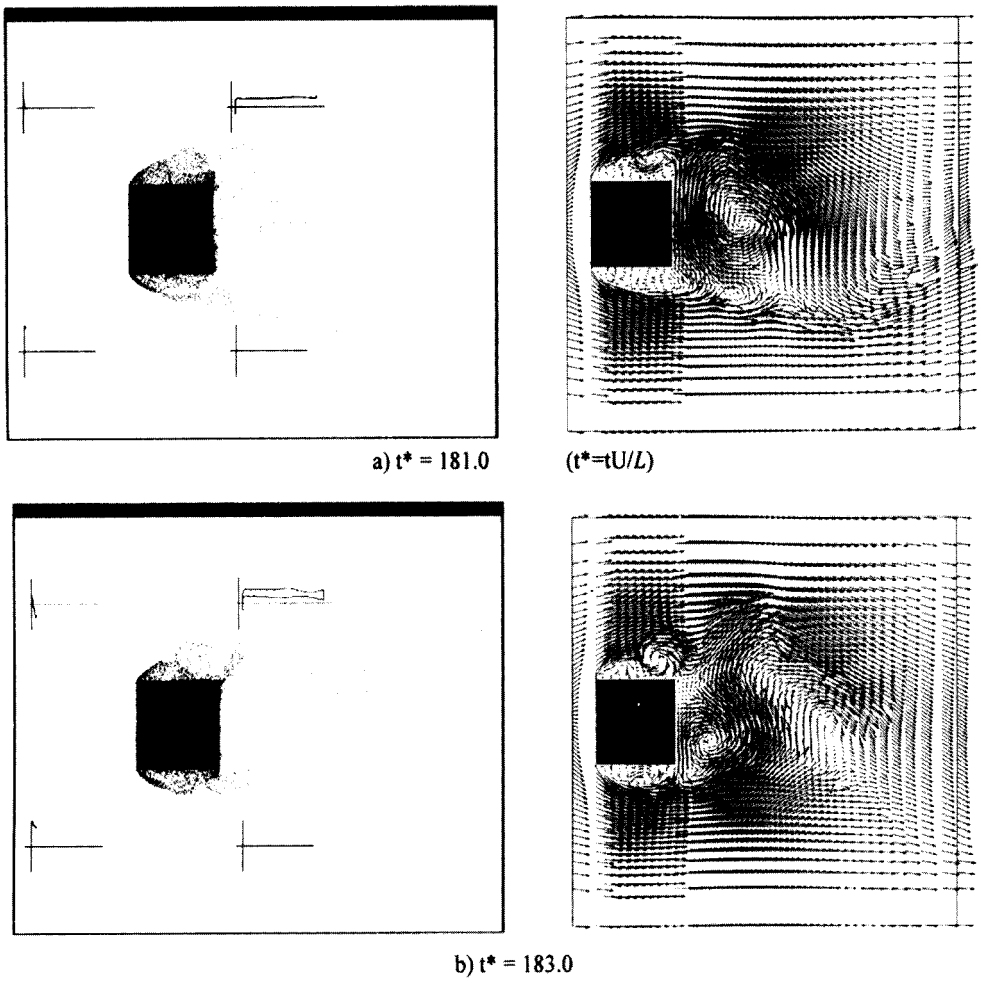

Fig. 4 Flow visualisation from DVM predictions for static square at 0° incidence

shed from corner D intermittently contacting corner C (Fig. 3a). Eventually, when α is approximately 15°, this shear layer reattaches completely to form a separation bubble on face DC. The shear layer that originally separated from D, now separates from C, giving rise to a narrower wake and a lower mean C_D. Further increases in α lead to an increase in the width of the wake, resulting in the gradual increase in C_D between 15° and 45°. The vortex method predicts this trend well, although the minimum C_D is predicted at 15° rather than the 12°-13° indicated in the experimental data.

The variation of C_L with incidence can also be explained by the reattachment of the shear layer to face DC. The separation bubble causes higher local suction pressures than those on face AB, which produce a negative lift coefficient, with a maximum at 15° when the shear layer is fully reattached. As the angle of incidence increases further, the separation bubble becomes smaller, so reducing the high local suction pressures on face DC, leading to a gradual increase in C_L. The results obtained from the vortex method again compare well with experimental data.

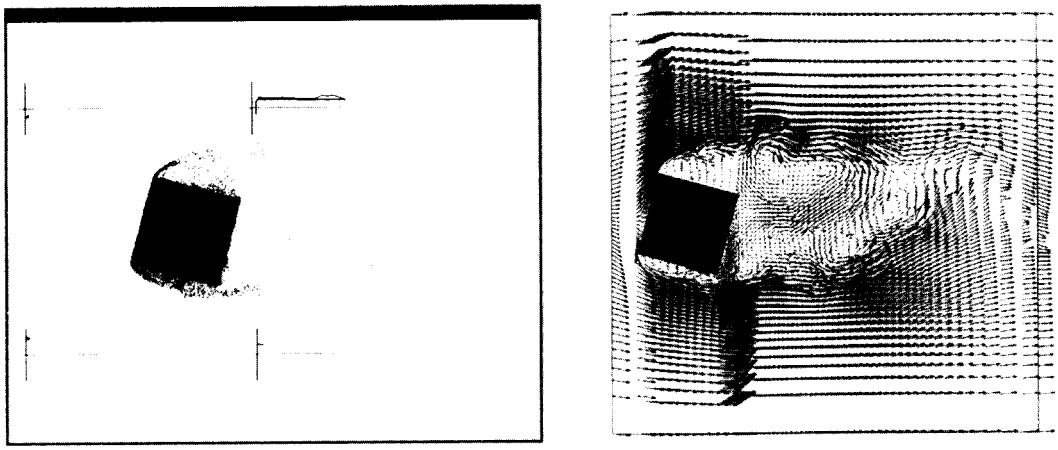

a) t* = 142.0

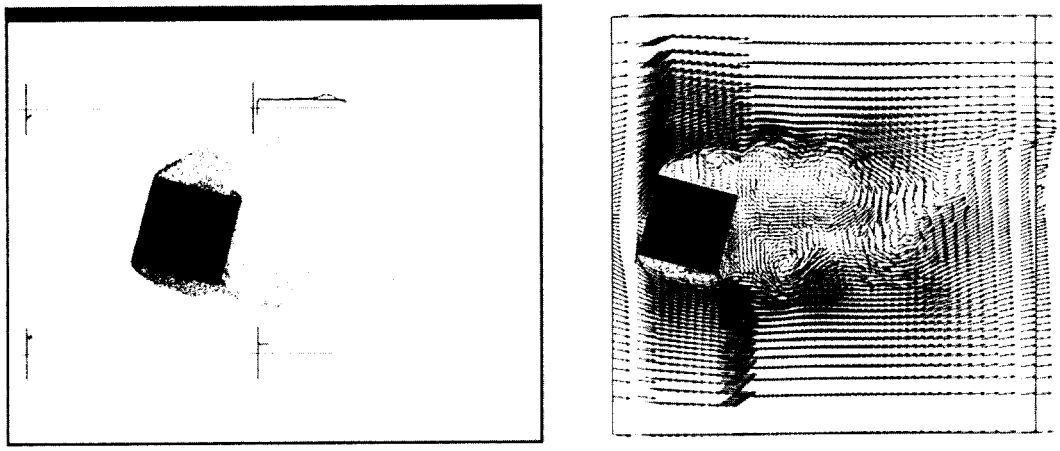

b) t* = 143.0

Fig. 5 Flow visualisation from DVM predictions for static square at 15° incidence

3.1.3. Strouhal number

Spectral analysis was performed on the time history of the lift coefficient, to obtain the Strouhal number, St:

$$St = n_s L / U \tag{12}$$

where n_s is the frequency of the vortex shedding. Due to the impulsive start to the calculation, the analysis was performed on a number of complete oscillation cycles of the lift history, after the flow had settled into a regular cycle of vortex shedding.

The variation of St with incidence is shown in Fig. 8, along with selected experimental data. The correct trends are predicted with a gradual increase in St until a peak is reached at approximately 20°. This is a little higher than experimental values, although a wide range of results has been presented by various researchers. The DVM overpredicts to some degree the vortex shedding frequency at the higher angles of incidence. However, the strength of the

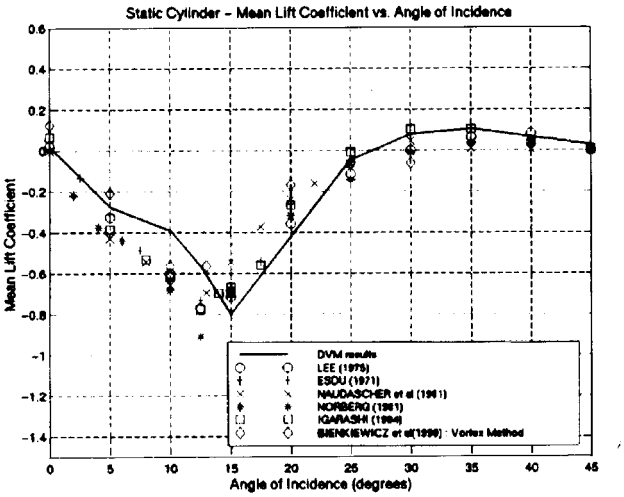

Fig. 6 Mean lift coefficient vs. incidence

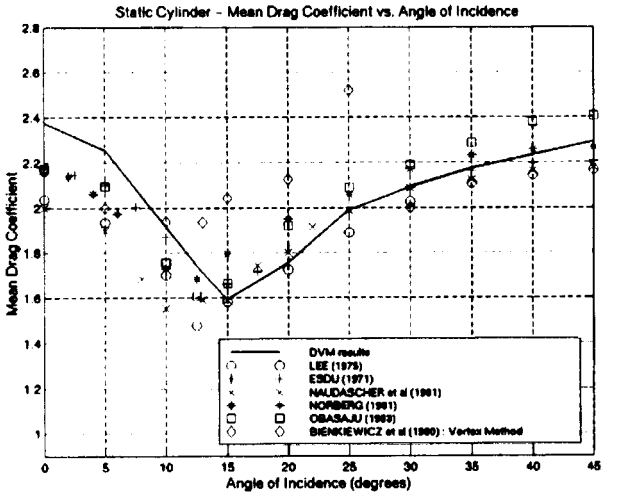

Fig. 7 Mean drag coefficient vs. incidence

vortex shedding and the resulting oscillation in the lift distribution is much weaker at the higher angles of incidence, giving rise to a wide range of values for *St*.

An interesting feature to note between 0° and 12° incidence, is that some researchers show a steady increase in *St* from 0° incidence, whereas others show a decrease in *St* before increasing to the peak value at approximately 13°. The reason for this behaviour is unclear, however in general terms a decrease in the width of the wake can be linked to an increase in *St*. The reattachment of the shear layer to the lower side face is the angle at which the wake is narrowest, and corresponds to the maximum *St* at 13°. In the cases where *St* initially decreases, the increase in the cross body dimension probably has most effect on the wake width, causing a wider wake. Whereas the gradual increase in *St* is probably more dependent on the intermittent reattachment of the shear layer at corner C (Fig. 3a). The wide range of results demonstrate the sensitivity of

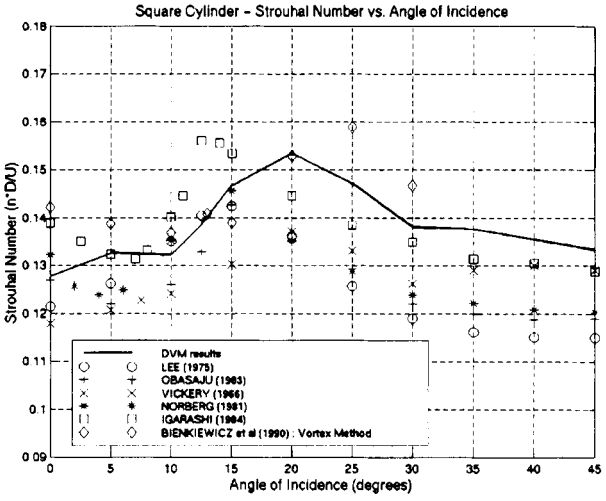

Fig. 8 Strouhal number vs. angle of incidence

St to the flow field, and emphasise the good quantitative agreement between the DVM and experiment.

3.1.4. Pressure coefficient on body surface

The pressure coefficient around the body for the 0° case is shown compared with experimental data, and with other computations in Fig. 9. The results are plotted against distance along the body surface, from the centre of the windward face and moving clockwise around the body, as shown in Fig. 3. The pressure coefficient is normalised using the pressure at the stagnation point as the reference pressure.

In general, good agreement is shown with experimental data, although the high suction on

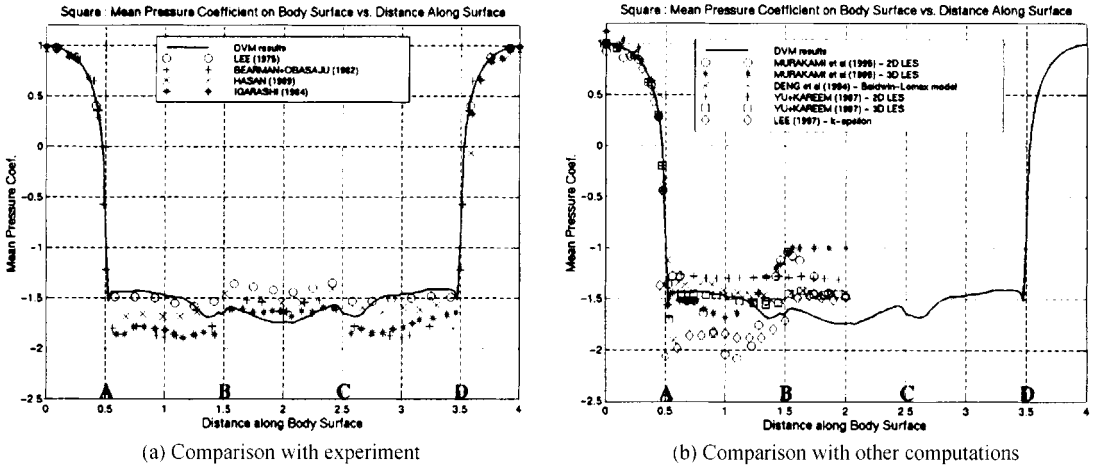

(a) Comparison with experiment (b) Comparison with other computations

Fig. 9 Surface pressure coefficient vs. distance along body surface

the leeward face is a symptom of the slightly high prediction of C_D at 0° The results also appear more favourable compared with those derived from both 2D and 3D CFD calculations. The discrepancy in the 2D CFD results can be attributed to the lack of modelling of the 3D effects in the wake, such as the development of streamwise component of vorticity, ω_x, due to the vortex stretching and roll up of the spanwise von Karman vortices. An empirical vortex decay model has been incorporated in the DVM to account for these 3D effects in the body wake (Taylor 1999). The results from the vortex method compare well with those calculated from full 3D methods, which use $O(10^5)$ grid points and which are also likely to be computationally much more expensive. From the high base pressure on the leeward face of the 3D CFD calculation from Murakami *et al.* (1995), the resulting mean drag coefficient is likely to be lower than experiment. Other methods also show discrepancies with experimental data, notably the high suction on the side face from the k-ε results of Lee (1997). However, the 3D CFD results of Yu *et al.* (1997) are generally in good agreement with the experimental data.

3.1.5. RMS fluctuating pressure coefficients

The rms lift coefficient for the 0° case was calculated to be 1.369. This compares well with experimental data, with various researchers giving values ranging between, 1.20 and 1.35.

The rms pressure fluctuations around the body surface are shown in Fig. 10 compared with various experimental data and with results from other computations. The vortex method results compare well with experiments, and on the side faces in particular, lies in the middle of a fairly wide range of results. The reduction of the fluctuations on the leeward face is also successfully predicted. The results from the 2D CFD calculations are quite poor, especially on the side face, whereas the 3D calculations all show generally good agreement with experiment. This can be attributed again to the 2D CFD method not taking account of the transfer of vorticity from the von Karman component due to 3D effects in the body wake. This is consistent with the results from the DVM, in that the predicted rms pressure fluctuations, particularly on the leeward face, were poor prior to the addition of the vortex decay model.

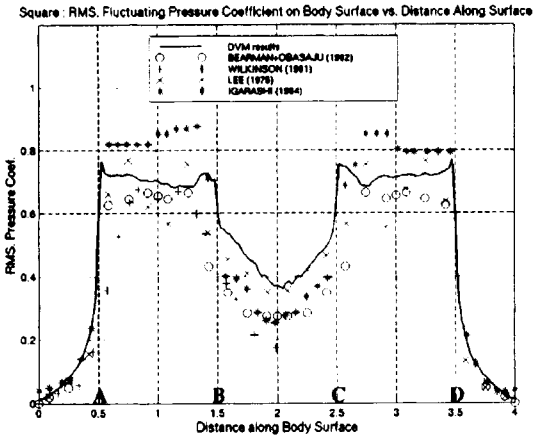

(a) Comparison with experiment

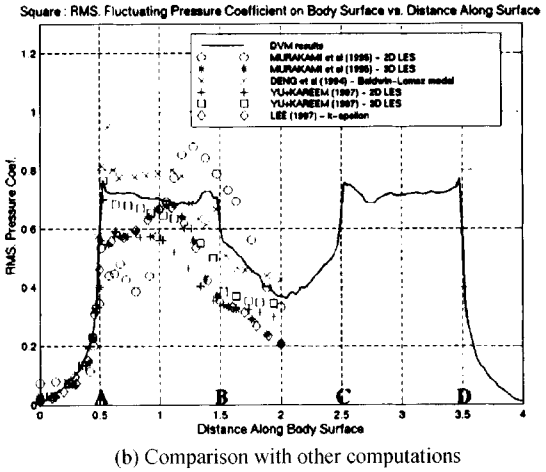

(b) Comparison with other computations

Fig. 10 Rms fluctuating pressure coefficient vs. distance along body surface

3.2. Oscillating square cylinder

The body motion is a forced sinusoidal oscillation with a fixed amplitude, usually presented as an amplitude ratio, a/L, where a is the amplitude of the oscillation and L is the side length of the square cylinder (Fig. 3b). The period of the body oscillation is represented non-dimensionally as a reduced velocity, U_r, defined as U/N_bL, where U is the freestream velocity and N_b is the frequency of the body oscillation. Results are presented for oscillations in the transverse direction for various amplitude ratios, with reduced velocities typically between 4.0 and 11.0.

The strong dependency of the flow field on the amplitude ratio and reduced velocity, leads to three distinct flow regimes, namely vortex lock-in, below lock-in and above lock-in. Above lock-in, the flow approaches quasi steady form as the dominance of the forcing oscillation diminishes. Below lock-in, the flow is dominated by the effects of the imposed oscillation and, depending on amplitude, the concentrated vorticity which is generated at the shedding frequency can lead to a complete suppression of the natural vortex shedding mode. Lock-in is defined as the reduced velocity range around the resonant frequency (St for the stationary cylinder is 0.128 from DVM results, Fig. 8) when the natural vortex shedding frequency transfers to the body frequency. These different flow states can be discerned from the time history of the lift coefficient and are discussed in detail in Taylor (1999). In the lock-in range, the lift history is close to sinusoidal, with only one dominant frequency present and with very little modulation of the amplitude of the lift coefficient. Below vortex lock-in, the lift history is quite irregular with a significant modulation of the amplitude, whereas, above lock-in, the quasi steady nature of the flow is noticeable.

3.2.1. Vortex shedding frequency measurements

Spectral analysis was performed on the lift histories with the results being used to ascertain the reduced velocity range at which vortex lock-in occurs for each amplitude ratio. Away from lock-in, the vortex shedding frequency and the body frequency can be seen as two distinct peaks in the frequency analysis. At vortex lock-in, the shedding frequency is modulated to the body frequency, and a single peak is seen in the frequency analysis (Taylor 1999).

The vortex shedding frequency, n_s, is estimated from these power spectra, and is shown, divided by the body frequency, N_b, plotted against U_r in Fig. 11 for an amplitude ratio of 0.1. The straight lines in the figures show the ratio between the St of the stationary body and N_b. Outside of vortex lock-in, the ratio n_s/N_b should be approximately on this line. In the lock-in region, the ratio becomes equal to unity as the shedding frequency is transferred to the body frequency. This is clearly demonstrated in the results from the DVM. Compared with experimental data (Bearman *et al.* 1982 and Otsuki *et al.* 1974), the region of vortex lock-in is well predicted for an amplitude ratio of 0.1. The width of the lock-in region increases at larger amplitude ratios and is also well predicted by the DVM (Taylor 1999).

3.2.2. General flow field visualisation

The flow field around the oscillating body is presented (Figs. 12 and 13) at the same stage of the oscillatory cycle, on consecutive cycles, for the reduced velocities $U_r = 6.0$, below vortex lock-in, and $U_r = 8.0$, in vortex lock-in. The results are shown as velocity vectors and

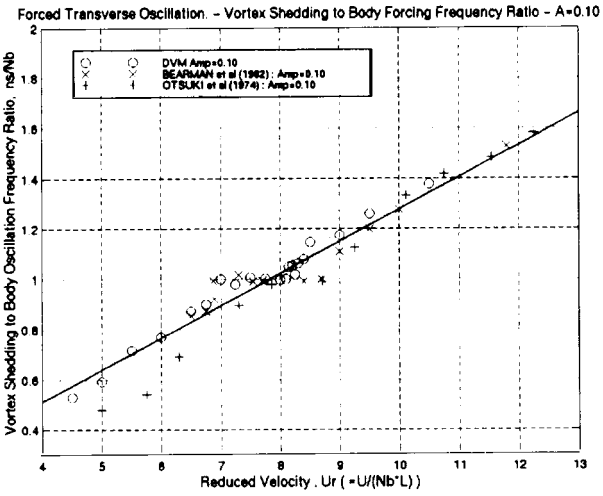

Fig. 11 Vortex shedding to body oscillation frequency ratio - Amp. Ratio = 0.1

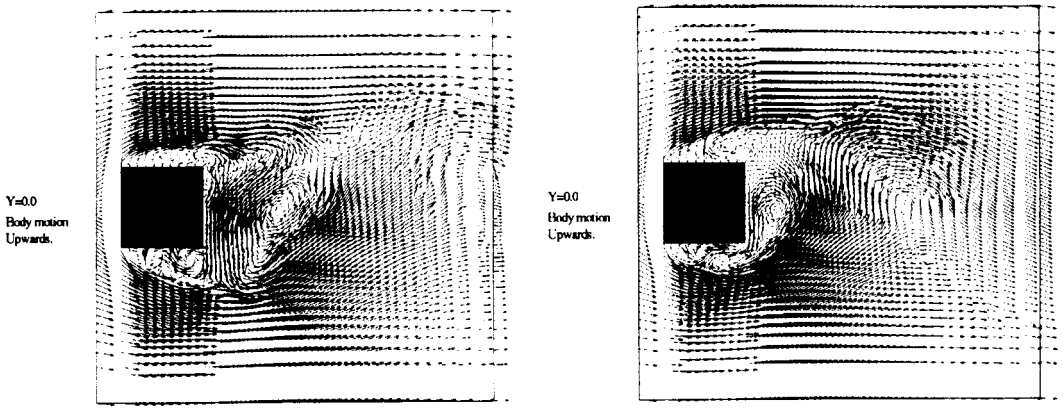

(a) t*=192.0 (b) t*=193.5

Fig. 12 Square cylinder with transverse oscillation, $U_r = 6.0$. (Below lock-in)
(Note - Body is at same stage in oscillation cycle in both figures)

in general provide good qualitative representations of the flow field. Compared to the results on a static square a much greater modulation of the wake is clearly discernible.

In the $U_r = 8.0$ case, the vortex shedding frequency is quite clearly the same as the body frequency demonstrating the vortex lock-in phenomena. This is apparent in Fig. 13, where the body is at the same stage of the oscillation cycle. In both cases, a vortex is forming close to the rear face, due to the shear layer that is shed from the lower side face. If the same comparison is made in Fig. 12, it is clear that vortex shedding occurs at a different frequency to the body oscillation, as illustrated by the dissimilar stages of the shedding cycle.

3.2.3. RMS lift coefficient, C_{Lrms}

The variation of the rms lift coefficient, C_{Lrms}, with U_r over a range of amplitudes is

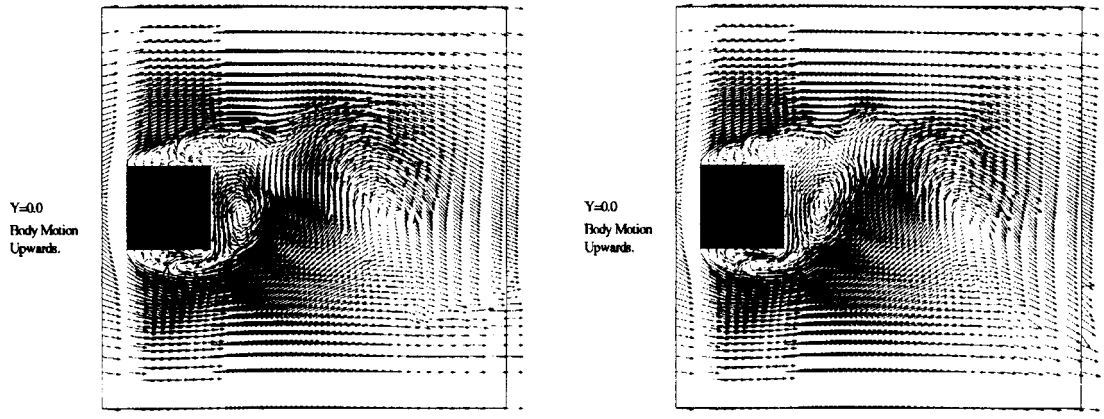

(a) t*=184.0 (b) t*=192.0

Fig. 13 Square cylinder with transverse oscillation, $U_r = 8.0$ (Vortex lock-in)

compared with experimental data (Lu *et al.* 1996 and Bearman *et al.* 1988) in Fig. 14. The variation of C_{Lrms} can be explained by considering the different flow regimes. At low U_r, below lock-in, concentrated vorticity is generated and shed at the body frequency, resulting in the natural vortex shedding mode being suppressed. This leads to a reduction in the fluctuating lift force on the body, an effect which is magnified with increasing oscillation amplitude. In the lock-in region, C_{Lrms} gradually increases until the maximum value is reached at the resonance point. Just above lock-in, the sharp decrease in the C_{Lrms} corresponds with the separation of the vortex shedding and body frequencies. An interaction occurs between the vortex formation and the rear corners on the square which reduces the strength of the vortex, producing the decrease in C_{Lrms}. As U_r is increased further, the flow approaches a quasi steady form, with C_{Lrms} gradually approaching the value found on the stationary body (equal to 1.37 in the DVM and 1.12 in Lu *et al.* 1996 (section 3.1.5)).

The results from the DVM demonstrate the variation discussed above and show generally

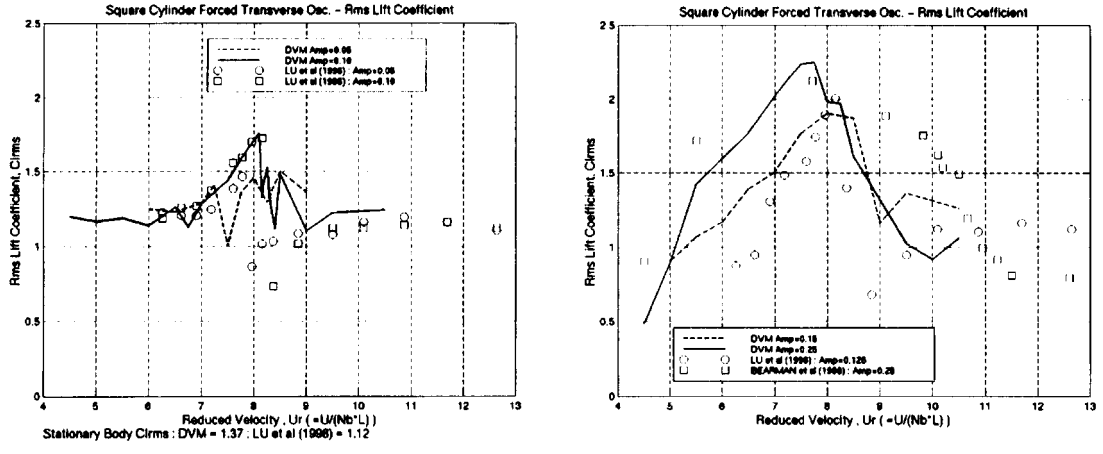

(a) Amplitude ratio=0.05 (b) Amplitude ratio=0.15

Fig. 14 Variation of rms lift coefficient with reduced velocity

good agreement with experimental data. It should be noted that some of the discrepancies can be attributed to the differences in the range of U_r for which lock-in is assumed. For example, the 0.25 amplitude ratio case has a lock-in range of approximately $U_r = 5.5$ to 12.0 in the experiments (Bearman *et al.* 1982 & 1988), whereas the DVM lock-in range is from 4.5 to 9.0. It can be shown that the lock-in is somewhat sensitive to Reynolds number, with a larger range of U_r expected at lower values. The Re employed in the DVM was chosen to be representative of all the experimental data being used for comparison but differs from each dataset to some degree. The results for the lowest amplitude ratio, 0.05, are more difficult to interpret as only a very small lock-in region was predicted at $U_r \approx 7.5$. Also, the vortex shedding is more dominant making the effects of body oscillation sometimes difficult to detect.

3.2.4. Phase angle and frequency-response component of lift

The phase angle, ϕ, is defined as the angle by which the lift force leads the body displacement. From this definition, the lift is capable of sustaining free oscillations of a spring mounted cylinder, when ϕ is within the range $0^\circ < \phi < 180^\circ$, the so called negative damping condition. The most noticeable feature is the sudden increase from negative to positive phase angle through the lock-in region. It is clear that positive ϕ required for vortex induced oscillations only occurs once the reduced velocity is above the resonance point. The slope of the phase angle distribution also tends to decrease with increasing amplitude, giving further indication of the increased lock-in range at higher amplitude.

The results from the DVM demonstrate good agreement with experimental data (Fig. 15), although these data show a wide variation, highlighting the sensitive nature of the unsteady flow field. In particular, the data from Nakamura *et al.* (1975) shows a noticeable difference to the phase angle results taken from other researchers (Fig. 15a). In addition, variations in the experimental flow conditions, such as Reynolds number, and variations in the static Strouhal number, may have had a strong effect on the results obtained from the oscillatory tests. However, the DVM results are within the range of experimental data, with the only discrepancy being the smaller predicted lock-in range at higher amplitudes discussed earlier. A favourable comparison can also be made with results obtained from a 3D CFD method (Murakami & Mochida 1995) at amplitude ratios of 0.10 and 0.25.

The component of the lift history at the body frequency, or "frequency-response" component, may be expressed as

$$L_b(t) = L_0 \cos(2\pi N_b t + \phi) \tag{13}$$

where L_0 is the amplitude of the frequency-response component. This may be non-dimensionalised to give the frequency-response component of the lift coefficient as given in Eq. (14)

$$C_{Lb}(t) = C_{L0} \cos(2\pi N_b t + \phi) \tag{14}$$

where

$$C_{L0} = \frac{L_0}{\frac{1}{2}\rho U^2 L} \tag{15}$$

is the amplitude of the frequency response component of the lift coefficient. C_{Lb} can be

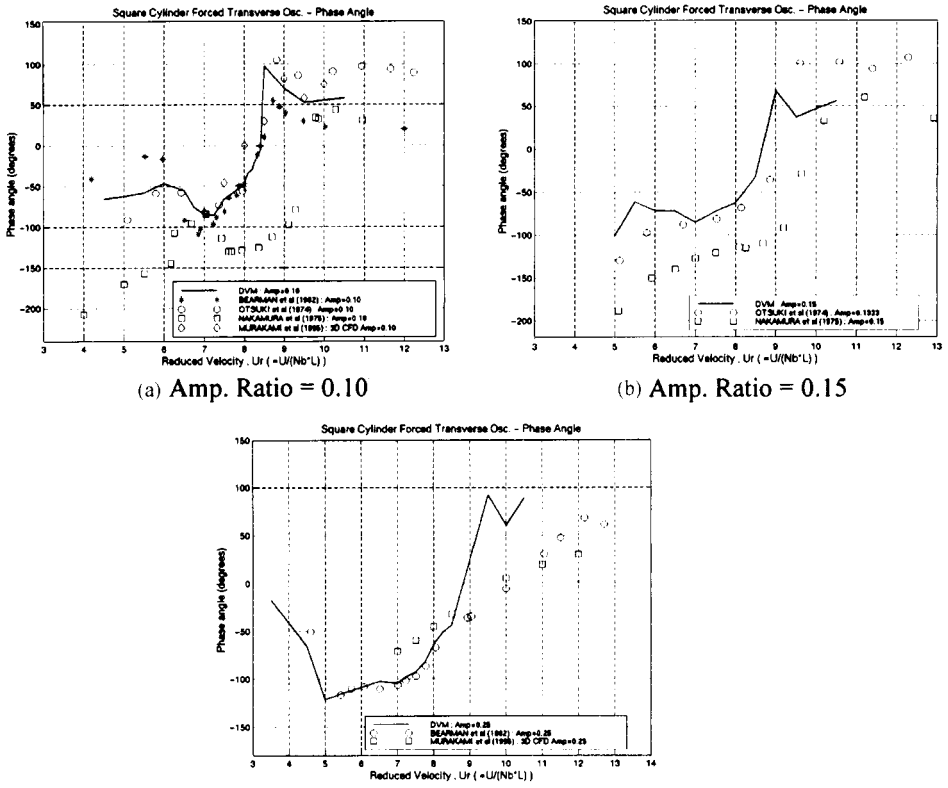

(a) Amp. Ratio = 0.10 (b) Amp. Ratio = 0.15

(c) Amp. Ratio = 0.25

Fig. 15 Phase angle, ϕ: Square cylinder with transverse oscillation

written in complex notation

$$C_{Lb}(t) = \mathrm{Re}\left[(C_{Lb\mathrm{R}} + iC_{Lb\mathrm{I}}) \exp(i 2\pi N_b t)\right] \tag{16}$$

where $C_{Lb\mathrm{R}}$ and $C_{Lb\mathrm{I}}$ are the real and imaginary components of the amplitude of the frequency-response part of the lift coefficient. These complex components can obtained from Eqs. (14) and (15)

$$\begin{aligned} C_{Lb\mathrm{R}} &= C_{L0} \cos\phi \\ C_{Lb\mathrm{I}} &= C_{L0} \sin\phi \end{aligned} \tag{17}$$

It may be noted that the condition that is required to enable vortex induced oscillation, is for $C_{Lb\mathrm{I}}$ to be positive.

Comparisons of the frequency response amplitude, C_{L0}, with various experimental data are shown in Fig. 16. The most noticeable feature of the results is the approximate correspondence of the peak C_{L0} with the resonance point, and the increasing peak value with amplitude. The DVM results demonstrate good agreement with the experimental results of Otsuki *et al.* (1974). As with the phase angle results, the data of Nakamura *et al.* (1975) gives very different results leading to uncertainties about the reliability of this data. Another feature to be noted is the C_{L0} values below lock-in tend to be higher than those above lock-in. This is indicative of the body oscillation

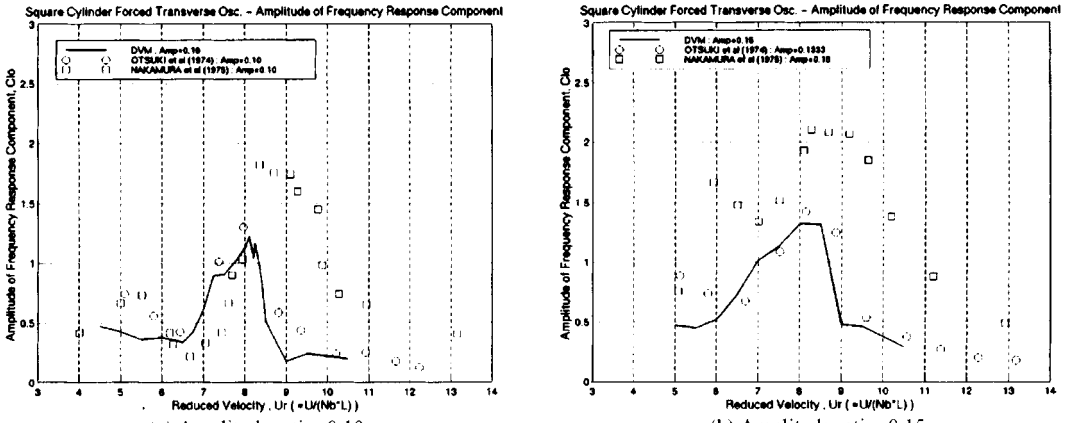

(a) Amplitude ratio=0.10 (b) Amplitude ratio=0.15

Fig. 16 Amplitude of frequency response component of lift coefficient

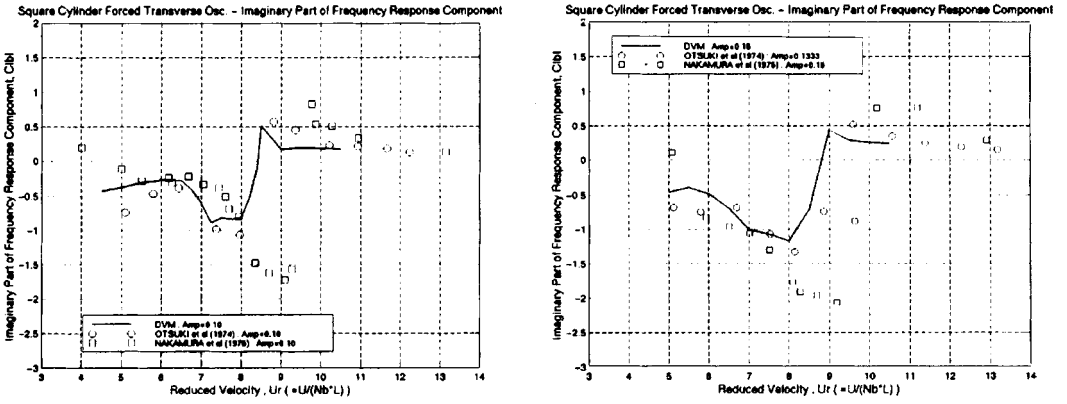

(a) Amplitude ratio=0.10 (b) Amplitude ratio=0.15

Fig. 17 Imaginary part of frequency response component of lift coefficient

having a more dominant effect on the lift force at the higher frequencies.

Good agreement between the DVM results for C_{Lbl} and experiments have also been obtained (Fig. 17). Again, comparison is affected by the large variation in different experimental results. The results show that the value of U_r at which C_{Lbl} becomes positive increases with amplitude as found in experiments. Allowing for differences in the experimental results, the reduced velocity at which C_{Lbl} becomes positive is also well predicted.

4. Conclusions

A Discrete Vortex Method (DVM) has been successfully developed at the Department of Aerospace Engineering, University of Glasgow. The method is based on the discretisation of the vorticity field into vortex particles which are shed from the body surface and tracked in the flow field in a Lagrangian manner.

The DVM has been successfully used to predict the flow field around static and oscillating

square section cylinders. In the static case, the results show good agreement with experimental data for mean force coefficients, Strouhal number and surface pressure coefficients. Also, the variation of these quantities with angle of incidence is demonstrated in the results of the DVM. The results also compare favourably with other computational methods.

The resonance phenomena of vortex lock-in is demonstrated in the results for the square section cylinder undergoing forced transverse oscillation. Results show good agreement with experimental data for the lock-in range, as well as phase angle. The trend of these quantities at different amplitudes and reduced velocities are demonstrated in the results of the DVM.

These results continue a successful validation programme and further enhance the capability of the DVM. Future research is aimed at using the DVM to analyse a wider range of geometries relevant to the field of wind engineering, such as suspension bridge deck sections. Also intended for future research is the inclusion of a dynamic solver, to enable full analysis of aeroelastic problems. In summary, the results obtained thus far on both static and oscillating bodies, indicate that the DVM developed at the University of Glasgow is becoming a powerful tool for determining the sectional aerodynamic and aeroelastic characteristics of bodies, typical of those found in the field of wind engineering.

Acknowledgements

The support and funding of this research by the Engineering and Physical Sciences Research Council (EPSRC) is gratefully acknowledged.

References

Bearman, P.W. and Obasaju, E.D. (1982), "An experimental study of pressure fluctuations on fixed and oscillating square-section cylinders", *Jl. Fluid Mech.*, **119**, 297-321.

Bearman, P.W. and Luo, S.C. (1988), "Investigation of the aerodynamic instability of a square-section cylinder by forced oscillation", *Jl. Fluids Struc.*, **2**, 161-176.

Bergstrom, D.J. and Wang, J. (1997), "Discrete vortex method of flow over a square cylinder", *Jl. Wind Eng. Ind. Aerodyn.*, **67-68** 37-49, *Proc. 2nd Int. Conf. on CWE (CWE 96)*, Fort Collins, Colorado, USA, 4-8 Aug. 1996.

Bienkiewicz, B. and Kutz, R.F. (1990), "Applying the discrete vortex method to flow about bluff bodies", *Jl. Wind Eng. Ind. Aerodyn.*, **36**, 1011-1020.

Bienkiewicz, B. and Kutz, R.F. (1993), "Aerodynamic loading and flow past bluff bodies using discrete vortex method", *Jl. Wind Eng. Ind. Aerodyn.*, **46-47**, 619-628.

Carrier, J., Greengard, L. and Rokhlin, V. (1988), "A fast adaptive multipole algorithm for particle simulations", *SIAM Jl. Sci. Stat. Comp.*, **9**, 669-686.

Chorin, A.J. (1973), "Numerical study of slightly viscous flow", *Jl. Fluid Mech.*, **57**, 785-796.

Clarke, N.R. and Tutty, O.R. (1994), "Construction and validation of a discrete vortex method for the two-dimensional incompressible navier-stokes equations", *Computers and Fluids*, **23**(6) 751-783.

Deng, G.B., Piquet, J., Queutey, P. and Visonneau, M. (1994), "2-D computations of unsteady flow past a square cylinder with baldwin-lomax model", *Jl. Fluids Struc.*, **8**, 663-680.

Esdu (1971), "Fluid forces, pressures and moments on rectangular blocks", *Engineering Sciences Data Item Number 71016.*

Hasan, M.A.Z. (1989), "The near wake structure of a square cylinder", *Int. Jl. Heat Fluid Flow*, **10**(4) 339-348.

Igarashi, T. (1984), "Characteristics of the flow around a square prism", *Bulletin of the JSME*, **27**(231) 1858-1865.

Koumoutsakos, P. and Leonard, A. (1995), "High-resolution simulations of the flow around an impulsively started ylinder using vortex methods", *Jl. Fluid Mech.*, **296**, 1-38.
Lee, B.E. (1975), "The effect of turbulence on the surface pressure field of a square prism", *Jl. Fluid Mech.*, **69**(2) 263-282.
Lee, S. (1997), "Unsteady aerodynamic force prediction on a square cylinder using k-ε turbulence models", *Jl. Wind Eng. Ind. Aerodyn.*, **67-68**, 79-90.
Leonard, A. (1980), "Vortex methods for flow simulation", *Jl. Comp. Phys.*, **37**, 289-335.
Lin, H. and Vezza, M. (1996), "A pure vortex method for simulating unsteady, incompressible, separated flows around static and pitching aerofoils", *Proc. 20th ICAS Conf.*, Sorrento, Italy, 8-13 September 1996, 2184-2193.
Lin, H., Vezza, M. and Galbraith, R.A.McD. (1997a), "Discrete vortex method for simulating unsteady flow around pitching aerofoils", *AIAA Jl.*, **35**(3), 494-499.
Lin, H. (1997b), "Prediction of separated flows around pitching aerofoils using a discrete vortex method", *Ph.D. Thesis, Dept. of Aerospace Engineering, University of Glasgow, Scotland, UK.*
Lu, P.C., Chen, R.H., Cheng, C.M. and Huang, J.H. (1996), "Aerodynamics of a vibrating square prism in homogenous turbulent flows", *Jl. Chinese Inst. Engs.*, **19**(3), 353-361.
Murakami, S. and Mochida, A. (1995), "On turbulent vortex shedding flow past 2D square cylinder predicted by CFD", *Jl. Wind Eng. Ind. Aerodyn.*, **54-55**, 191-211.
Nakamura, Y. and Mizota, T., (1975), "Unsteady lifts and wakes of oscillating rectangular prisms", *Jl. Eng. Mech. Div., ASCE* **101**, 855-871.
Naudascher, E., Weske, J.R. and FEY, B. (1981), "Exploratory study on damping of galloping vibrations", *Jl. Wind Eng. Ind. Aerodyn.*, **8**, 211-222.
Norberg, C. (1993), "Flow around rectangular cylinders : Pressure forces and wake frequencies", *Jl. Wind Eng. Ind. Aerodyn.*, **49**(1-3), 187-196.
Obasaju, E.D. (1983), "An investigation of the effects of incidence on the flow around a square section cylinder", *Aero. Quarterly*, **34**, 243-259.
Otsuki, Y., Washizu, K., Tomizawa, H. and Ohya, A. (1974), "A note on the aeroelastic instability of a prismatic bar with square cross section", *Jl. Sound Vib.*, **34**(2), 233-248.
Puckett, E.G. (1993), "Vortex methods : An introduction and survey of selected research topics", *Incompressible Computational Fluid Dynamics*, (ed. M.D. Gunzburger and R.A. Nicolaides), Cambridge University Press.
Sarpkaya, T. (1989), "Computational methods with vortices - The 1988 freeman scholar lecture", *Jl. Fluids Eng.*, **111**, 5-52.
Taylor, I.J. and Vezza, M. (1997), "Application of a zonal decomposition algorithm, to improve the computational operation count of the discrete vortex method calculation", *G.U. Aero Report No. 9711*, Dept. of Aerospace Engineering, University of Glasgow, Scotland, UK.
Taylor, I.J. (1999), "Study of bluff body flow fields and aeroelastic stability using a discrete vortex method", Ph.D. Thesis, Dept. of Aerospace Engineering, University of Glasgow, Scotland, UK. (Submitted for examination January 1999).
Vickery, B.J. (1966), "Fluctuating lift and drag on a long cylinder of square cross-section in a smooth and in a turbulent stream", *Jl. Fluid Mech.*, **25**(3), 481-494.
Vezza, M. (1992), "A new vortex method for modelling two-dimensional, unsteady incompressible, viscous flows", *G.U. Aero Report No. 9245*, Dept. of Aerospace Engineering, University of Glasgow, Scotland, UK.
Walther, J.H. and Larsen, A. (1997), "Two dimensional discrete vortex method for application to bluff body aerodynamics", *Jl. Wind Eng. Ind. Aerodyn.* **67-68** 183-193. *Proc. 2nd Int. Conf. on CWE (CWE 96)*, Fort Collins, Colorado, USA, 4-8 Aug. 1996.
Wilkinson, R.H. (1981), "Fluctuating pressures on an oscillating square prism. Part 1 : Chordwise distribution of fluctuating pressure", *Aero. Quarterly*, **32**(2). 97-110.
Yu, D. and Kareem, A. (1997), "Numerical simulation of flow around rectangular prism", *Jl. Wind Eng. Ind. Aerodyn.*, **67-68**, 195-208.

(*Communicated by Giovanni Solari*)